CHEMICAL PHYSICS

Graphene catalyzes the reversible formation of a C–C bond between two molecules

J. J. Navarro[1,2]*, M. Pisarra[2,3]*, B. Nieto-Ortega[2], J. Villalva[2], C. G. Ayani[2], C. Díaz[3,4,5], F. Calleja[2], R. Miranda[1,2,5], F. Martín[2,3,5], E. M. Pérez[2]†, A. L. Vázquez de Parga[1,2,5]†

Carbon deposits are well-known inhibitors of transition metal catalysts. In contrast to this undesirable behavior, here we show that epitaxial graphene grown on Ru(0001) promotes the reversible formation of a C–C bond between $-CH_2CN$ and 7,7,8,8-tetracyano-*p*-quinodimethane (TCNQ). The catalytic role of graphene is multifaceted: First, it allows for an efficient charge transfer between the surface and the reactants, thus favoring changes in carbon hybridization; second, it holds the reactants in place and makes them reactive. The reaction is fully reversible by injecting electrons with an STM tip on the empty molecular orbitals of the product. The making and breaking of the C–C bond is accompanied by the switching off and on of a Kondo resonance, so that the system can be viewed as a reversible magnetic switch controlled by a chemical reaction.

INTRODUCTION

Deposits of graphitic carbon act as poisons of transition metal catalysts (*1*) due to their chemical inertness and physical blockage of the catalyst active sites (*2*, *3*). How to avoid this poisoning has thus become an active field of research (*4*, *5*), mostly under the controlled environment of single crystals in ultrahigh vacuum (UHV), which provides the ideal conditions to study the active part of heterogeneous catalysis (*6*–*8*). For this very reason, the study of graphitic carbon monolayers grown on different metallic substrates started well before the isolation of graphene (*9*–*11*).

Nowadays, there are well-established procedures to obtain high-quality large areas of graphene sheets epitaxially grown on transition metal surfaces, e.g., via catalytic cracking of carbon-containing gases or carbon segregation from the bulk (*11*–*13*). Experimental and theoretical work performed on these systems has shown that the interaction between graphene and the metallic substrate can be tuned by carefully choosing the metal, thus opening a way to tailor the properties of graphene. A similar control of graphene properties can be achieved through chemical functionalization. By selecting suitable molecules, one can engineer graphene bandgaps (*14*), control its doping level (*15*), or add magnetic functionalities (*16*).

Graphene monolayers can also be used to isolate molecules from the strongly interacting metallic substrates, thus preventing the formation of hybridized metal-molecule orbitals. Accordingly, the graphene-metal interface is an ideal playground to explore the mutual interaction between unperturbed organic molecules in two dimensions (*17*), to achieve the growth of three-dimensional molecular crystals (*18*), or to study unperturbed molecular orbitals (*19*). Furthermore, graphene can also favor charge transfer from the metal to the adsorbed molecules, leading to the formation of radical ions with chemical properties that are usually different from those of their gas phase counterparts.

In this work, we show that a nanostructured graphene monolayer epitaxially grown on Ru(0001) promotes a chemical reaction that would hardly take place under noncatalyzed conditions. The graphene layer promotes the reversible formation of a C–C bond between cyanomethylene groups ($-CH_2CN$), fixed by covalent bonds at specific positions on the graphene surface, and 7,7,8,8-tetracyano-*p*-quinodimethane (TCNQ), physisorbed on the graphene and therefore able to diffuse at room temperature. Upon reaction, the resulting product has the cyanomethylene group on top of the TCNQ and pointing to the vacuum covalently bonded to one of the exocyclic alkenes of the TCNQ, while the TCNQ remains physisorbed on the surface. By means of low-temperature scanning tunneling microscopy (LT-STM)/spectroscopy (LT-STS) in UHV and density functional theory (DFT) calculations, we characterize the resulting TCNQ-CH_2CN molecule. Single-molecule manipulation, using the STM tip to inject electrons in the lowest unoccupied molecular orbital (LUMO) of the TCNQ-CH_2CN, results in the breaking of the C–C bond and the recovery of the reactants.

RESULTS AND DISCUSSION

Graphene monolayers can be epitaxially grown on many single-crystal metal surfaces under UHV conditions. These monolayers protect highly reactive metallic surfaces from contaminants. Using the appropriate parameters (see Materials and methods), we make sure that the metallic surface is completely covered with a continuous graphene layer (see section S1) (*20*). Because of the difference in lattice parameters between the metallic substrates and graphene, a new super periodicity appears on the surface, the so-called moiré pattern. In this way, the graphene layers are naturally nanostructured with a periodicity of the order of 2 to 3 nm (*11*–*13*). This new periodicity modulates the registry between carbon and metal atoms (*20*–*22*) and, therefore, modulates the electronic properties of graphene (see section S1) (*23*, *24*). Taking advantage of this fact, a graphene-Ruthenium (gr-Ru) surface has been functionalized with cyanomethylene groups with high yield and extreme spatial selectivity (*25*, *26*). The functionalized surface presents a long-range spatial arrangement of cyanomethylene groups, $-CH_2CN$, covalently bonded to the center of the hexagonal closed-packed (HCP)–top areas in the moiré unit cell (green triangles in Fig. 1A) with a periodicity of 2.9 nm.

[1]Dep. Física de la Materia Condensada, Universidad Autónoma de Madrid, Cantoblanco, 28049 Madrid, Spain. [2]IMDEA Nanociencia, Calle Faraday 9, Cantoblanco, 28049 Madrid, Spain. [3]Dep. Química Módulo 13, Universidad Autónoma de Madrid, Cantoblanco, 28049 Madrid, Spain. [4]Institute for Advanced Research in Chemistry (IAdChem), Universidad Autónoma de Madrid, Cantoblanco, 28049 Madrid, Spain. [5]Condensed Matter Physics Center (IFIMAC), Cantoblanco, 28049 Madrid, Spain.
*These authors contributed equally to this work.
†Corresponding author. Email: emilio.perez@imdea.org (E.M.P.); al.vazquezdeparga@uam.es (A.L.V.d.P.)

TCNQ is an electron acceptor molecule that has been used to p dope graphene films (*27*). When deposited on gr-Ru, the preferred adsorption area is between two ripples, the so-called bridge position, with two nitrile groups over the face centered cubic (FCC)–top area and the other two over the HCP-top (see Fig. 1B). LT-STM images and LT-STS maps show the spatial distribution of the molecular orbitals almost unperturbed (*16*, *17*). This is possible because of the low density of states and low reactivity of graphene, which prevents the hybridization of the TCNQ molecular orbitals with the metallic electronic states from the substrate. In contrast, when TCNQ is deposited directly on clean Ru(0001), the molecules appear in the STM images as bright protrusions showing no detail inside the molecule (see section S2). Simultaneously, the graphene overlayer allows for an efficient charge transfer from the Ru surface to the electron acceptor TCNQ. The reduced TCNQ core loses the quinoid character in favor of aromatization, while the exocyclic bonds present a sizable lengthening to accommodate the extra charge and acquire a radicaloid character (see section S3). This unpaired electron provides the TCNQ gr-Ru system with long-range magnetic order (*16*). Considering these precedents, we decided to investigate the adsorption of TCNQ molecules over gr-Ru previously patterned covalently with $-CH_2CN$ groups.

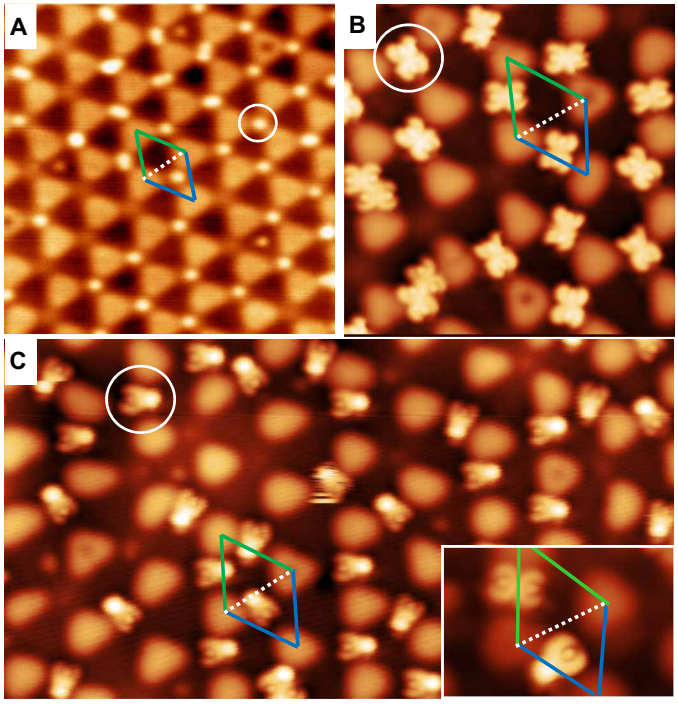

Fig. 1. CH_2CN and TCNQ deposited on gr-Ru(0001) before and after the reaction. (**A**) STM image [20 nm by 20 nm, sample bias voltage (V_b) = +1.7 V, tunneling current (I_t) = 10 pA] showing the gr-Ru surface with all the HCP-top areas (blue triangle) functionalized with $-CH_2CN$ groups. White circle indicates a single $-CH_2CN$. (**B**) STM image (12 nm by 12 nm, V_b = −0.8V, I_t = 25 pA) with TCNQ adsorbed on gr-Ru. Most of the TCNQ molecules are adsorbed in the so-called bridge positions. White circle indicates a single TCNQ. (**C**) STM image (27 nm by 15 nm, V_b = −1.5 V, I_t = 5 pA) showing the surface after the sequential deposition of $-CH_2CN$ groups followed by the TCNQ molecules at room temperature. All the TCNQ molecules present on the image have reacted with the $-CH_2CN$ groups. White circle indicates a reacted TCNQ. The inset shows an STM image (5.7 nm by 4.0 nm, V_b = −1.3V, I_t = 15 pA) with one pristine TCNQ molecule (top left) and a reacted one. The gr-Ru(0001) moiré pattern is visible in all the images. The blue (green) triangles highlight the HCP-top (FCC-top) parts of the moiré pattern. All images were measured at 4.8 K.

The STM images measured at 4.8 K after deposition of TCNQ on gr-Ru previously patterned with cyanomethylene groups show an unexpectedly new scenario, as can be seen in Fig. 1C. Almost all TCNQ molecules are modified, with one-half of the molecule unperturbed, preserving the intramolecular resolution obtained on pristine TCNQ, while in the other half, the intramolecular resolution is lost, and a bright protrusion is observed. The inset in Fig. 1C shows a high-resolution image of one pristine TCNQ and one modified TCNQ, demonstrating that the loss of the intramolecular resolution is not due to the STM tip or the acquisition parameters. A notable feature in the STM images is the disappearance of the cyanomethylene substituents from the graphene surface: Before the deposition of TCNQ, the cyanomethylenes were chemically bonded to the HCP-top areas of the moiré pattern, as shown in Fig. 1A, but after the deposition of the TCNQ molecules, the HCP-top areas are clean. Another interesting experimental fact is the strict order in the orientation of the modified TCNQ molecules: All of them are adsorbed on the bridge areas with the bright bump pointing toward the FCC-top areas (see Fig. 1C).

To identify the structure of the modified TCNQs, we have performed two different sets of DFT calculations (see Materials and methods and the Supplementary Materials). First, we have determined the possible configurations resulting from the combination of cyanomethylene and TCNQ in the gas phase and their thermodynamic stability (see section S4). The most stable configuration of the TCNQ-CH_2CN has the cyanomethylene group bonded to the C atom at the end of the exocyclic bond of the TCNQ (see Fig. 2, A and B). As can be seen in Fig. 2B, the TCNQ core of the product molecule is bent after the reaction because of the change in hybridization of the C atom bonded to the cyanomethylene.

Starting from the structure obtained in the gas phase (Fig. 2, A and B), we have investigated the adsorption configuration and the corresponding adsorption energy of the TCNQ-CH_2CN on the gr-Ru surface. In these DFT calculations, we have explicitly included the ruthenium substrate, the graphene monolayer, and the TCNQ-CH_2CN molecules. The simulated gr-Ru substrate accounts for the observed moiré pattern and provides an accurate representation of the geometry and electronic properties of this surface (*21*–*24*).

Figure 2 (C and D) shows the lowest energy configuration for the adsorption of the TCNQ-CH_2CN molecule on gr-Ru. As in the case of pristine TCNQ molecules (*16*, *28*), the new molecule is adsorbed on a bridge position. The asymmetry of the TCNQ-CH_2CN introduces a new coordinate to describe the adsorption geometry. The end of the TCNQ bonded to the cyanomethylene group points toward the FCC-top areas, in perfect agreement with the experimental data (see Fig. 1C and section S5). The proposed molecular structure of the TCNQ-CH_2CN is further supported by the excellent agreement between the measured (Fig. 3, A and B) and calculated (Fig. 3, C and D) STM images. To check the stability and resolution of the STM tip, the experimental images show a region containing an unreacted TCNQ.

All the above suggests that, after the chemical reaction, the cyanomethylene group, now detached from graphene, surfs the substrate on top of the TCNQ, with the latter dictating the final adsorption configuration. Our DFT calculations predict an adsorption energy of 3.1 eV (71.5 kcal mol^{-1}) for the most stable configuration shown in Fig. 2 (C and D). Differences in adsorption energies

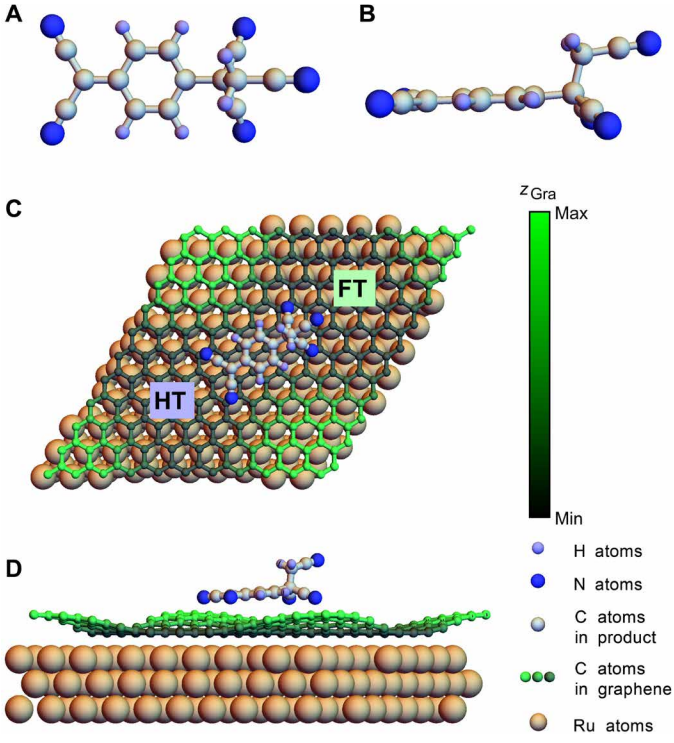

Fig. 2. DFT-calculated geometries. (**A**) Top view and (**B**) side view of the resulting molecule in the gas phase calculation: The cyanomethylene group is bonded to one of the exocyclic alkenes of the TCNQ. (**C**) Top view of the most stable adsorption configuration on the gr-Ru(0001). The molecule is adsorbed on the bridge position with the cyanomethylene end pointing toward the FCC-top areas (FT) of the moiré pattern. (**D**) Lateral view of the most stable configuration. The cyanomethylene group is located on top of the TCNQ and points toward the vacuum. In (C) and (D), the total corrugation of graphene is ~120 pm.

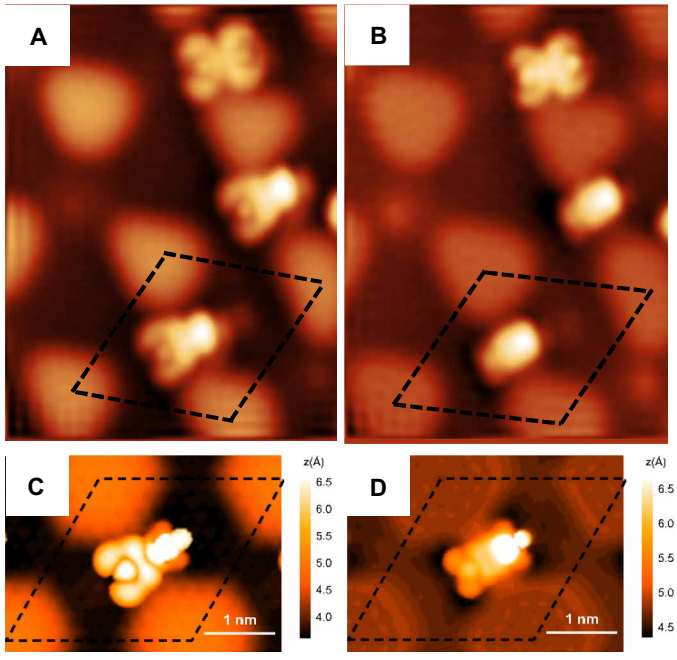

Fig. 3. STM images for positive and negative bias voltages. (**A**) STM image (6 nm by 8 nm) of two TCNQ-CH_2CN molecules and one TCNQ on gr-Ru for negative bias voltage (V_b = −1.7 V, I_t = 5 pA). Total corrugation in the image is 240 pm. (**B**) STM image (6 nm by 8 nm) of the same area of the sample shown in (A) acquired at positive bias voltage (V_b = +1.1V, I_t = 5 pA). Total corrugation in the image is 186 pm. (**C** and **D**) Simulated STM image of a TCNQ-CH_2CN on gr-Ru for (C) negative bias (V_b= −1.7 V, I_t = 5 pA) and (D) positive bias voltage (V_b = +1.1 V, I_t = 5 pA); the origin of the *z* scale is set on the *z* coordinate of the C atoms in the low region of the graphene moiré. The dashed black line rhombus in all the images indicates the moiré unit cell for gr-Ru.

between different configurations are as large as ~0.2 eV (4.6 kcal mol^{-1}), explaining why we exclusively find one adsorption configuration experimentally (see section S5). In the most stable configuration, the shortest distance between the TCNQ-CH_2CN and the graphene atoms is of the order of 3 Å, confirming that the molecule is physisorbed on the surface. The calculations also show that the charge transfer from the surface to the TCNQ-CH_2CN amounts to ~0.86 electrons, very similar to the charge transferred from the substrate to the pristine TCNQ (*16*, *29*).

It is worth stressing the important role of the surface, and of graphene particularly, in catalyzing the formation of the TCNQ-CH_2CN molecule (see section S6). The reaction of TCNQ with CH_3CN (the pristine reactants in the gas phase) leading to the TCNQ-CH_2CN molecule plus the loss of a hydrogen atom is very unlikely: The calculated energy barrier is ~5 eV (~114 kcal mol^{-1}). In contrast, as shown by the results of a simple model in which ruthenium atoms are ignored and the graphene layer is reduced to a few carbon atoms (see section S6 for details), the presence of the graphene layer reduces the energy barrier by a factor of 5, thus favoring the formation of the products. A similarly clean reaction is not possible on pristine Ru(0001) because on the one hand, the very reactive character of Ru leads to the adsorption of CH_3CN, $-CH_2CN$, and possibly other chemical species during the functionalization with $-CH_2CN$. And on the other hand, the reactivity hinders the mobility of TCNQ molecules once adsorbed on the Ru(0001) surface (see section S2). In turn, the Ru substrate locally modifies the chemical properties of the graphene layer, favoring the adsorption of $-CH_2CN$ on the HCP-top areas. Such a selectivity would be difficult to obtain by using conventional carbon.

The nanostructured epitaxial graphene monolayer promotes the reaction in a threefold way: First, it holds the $-CH_2CN$ groups in place and makes them reactive toward TCNQ by acting as a good leaving group; second, it allows for an efficient charge transfer from the ruthenium substrate, which thus acts as an electron reservoir during the chemical reaction; and last, it prevents the chemical reaction between the TCNQ and the Ru(0001) surface and allows the TCNQ to diffuse on the surface at room temperature (see section S2).

To investigate the consequences of this new chemical reaction on the electronic structure of the molecules, we performed spatially resolved *dI*/*dV* spectra in an area of the surface where pristine TCNQs and TCNQ-CH_2CN coexist. Figure 4 shows the *dI*/*dV* curves measured at 4.8 K on the individual TCNQ (blue trace) that appears in the image shown in the inset (blue circle). On the basis of previous results (*16*, *28*, *29*), the features in the spectrum can be assigned to the TCNQ molecular orbitals. The peak at −1.6 V corresponds to the highest occupied molecular orbital (HOMO), populated with two electrons. Because of the charge transfer from the substrate, the parent LUMO of the TCNQ is now populated with one electron, and therefore one of the spin components appears below the Fermi level (around −0.9 V), now called singly occupied molecular orbital

(SOMO). The other (unoccupied) spin component of the parent LUMO appears above the Fermi level (+1.0 V) and is called singly unoccupied molecular orbital (SUMO) (*16*, *28*, *29*). The *dI*/*dV* curve measured in the nearby TCNQ-CH_2CN (red trace and circle in Fig. 4) shows two peaks below the Fermi level, one at −1.8 V and the other at −1.2 V, and, between them, an energy region showing negative differential conductance (see also section S7). Above the Fermi level (up to +1.0 V), a steady increase of the signal is observed. These remarkable differences in the electronic structure are a direct indication of a change in the covalent structure of TCNQ after the reaction with the $-CH_2CN$ groups.

From our DFT calculations (see sections S8 and S9 for details), we can identify the origin of the peaks observed in the *dI*/*dV* spectra measured on the TCNQ-CH_2CN. The calculated projected density of states (pDOS) shows the presence of two peaks below and one peak above the Fermi level in an energy window of ±3 eV. From the comparison between the pDOS and the gas phase calculations, the *dI*/*dV* peak at lower energy (−1.8 V) can be attributed to the HOMO−1 orbital of the original TCNQ molecule. The other peak below the Fermi level, appearing at −1.2 V, can be associated with the former LUMO of TCNQ. After the reaction, two electrons occupy this molecular orbital, reflecting the formation of a new covalent bond (see section S9). This electronic state appears below the Fermi level and is the HOMO of the TCNQ-CH_2CN. According to the calculations, the LUMO of the TCNQ-CH_2CN appears at energies above +2.5 eV, explaining why it is not observed experimentally.

It is known that injection of electrons with an STM into unoccupied molecular orbitals may induce molecular motion (*30*), isomerization (*31*), or selective bond breaking (*32*). We analyze now what happens when electrons are injected into the TCNQ-CH_2CN. Figure 5A shows an STM image obtained by using a bias voltage of +1.7 V and a tunneling current of 10 pA. In the image, one can observe four unreacted cyanomethylene groups, chemically attached to the HCP-top areas of the graphene surface, and four TCNQ-CH_2CN molecules. The blurry appearance of the latter indicates that, under these conditions, the TCNQ-CH_2CN molecules move slightly around the adsorption position during the topographic image acquisition. In Fig. 5B, we show the STM topography, acquired with the same conditions on the same area, immediately after manipulating individually the four TCNQ-CH_2CN by positioning the STM tip on top of each one of them and setting the bias voltage to +2.0 V (see also section S10). The new topography shows that the former four TCNQ-CH_2CN molecules now look as pristine TCNQ, and three new $-CH_2CN$ groups are visible in the image (blue circles). It is worth noticing that the shape of the new $-CH_2CN$ groups is slightly different from that of the $-CH_2CN$ groups adsorbed on the HCP-top region (also compare with Fig. 1A) because of their bonding to a different adsorption site. This is possible because the experimental manipulation is carried out at 4.6 K, and hence, the $-CH_2CN$ radicals do not have enough energy to explore the surface and reach the HCP-top adsorption site where the adsorption energy is maximum (*25*, *26*). On the basis of the calculated pDOS, we can rationalize the manipulation process in the following way: Because of the high positive bias voltage (>+1.7 V), the tunneling electrons are injected into the tail of the LUMO of the TCNQ-CH_2CN. Since this is an antibonding orbital, the electrons induce the breaking of the C–C chemical bond, thus leading to the recovery of the initial reactants, CH_2CN-graphene and physisorbed TCNQ. As demonstrated in section S10, this manipulation process is reproducible and can be efficiently used to reverse the reaction at the single-molecule level.

According to our DFT calculations, a consequence of the chemical reaction between TCNQ and the cyanomethylene groups is the different occupancy of the molecular orbitals in the TCNQ-CH_2CN compared with pristine TCNQ (see also section S9). To investigate it, we resort to the appearance of a Kondo resonance in the STS data. The Kondo effect reflects the screening of the spin of magnetic impurities by the conduction electrons of nonmagnetic metals that results in a many-body ground state below the Kondo temperature, T_K (*33*). Consequently, a sharp feature is observed at the Fermi level in the LT-STS spectra recorded on top of magnetic impurities (*34*). A sharp peak appears if the magnetic impurity is weakly coupled to the substrate, as often occurs for adsorbed molecules with a magnetic moment (*35*).

Figure 6A shows the *dI*/*dV* spectra measured on a dimer formed by H bonding between a TCNQ and a TCNQ-CH_2CN adsorbed on

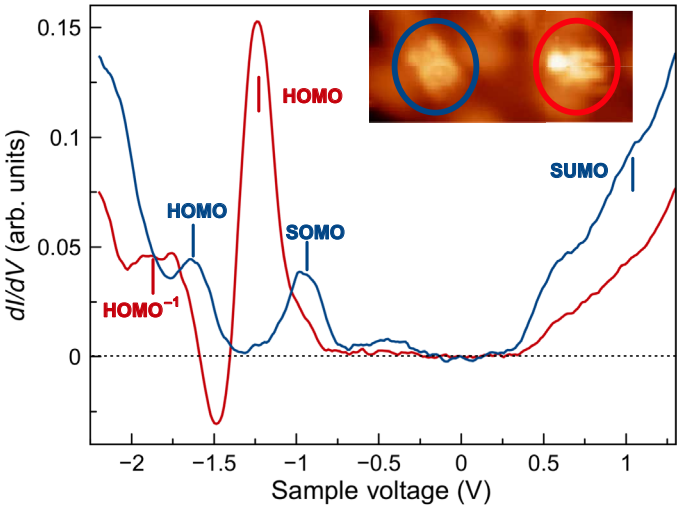

Fig. 4. TCNQ and TCNQ-CH_2CN molecular orbitals. STS spectra measured in the TCNQ molecule (blue circle and trace) and TCNQ-CH_2CN (red circle and trace). Both spectra have been measured at 4.8 K with a lock-in technique using a peak-to-peak modulation of 90 mV. The inset shows an STM image (8 nm by 3 nm, V_b = −2.2 V, I_t = 20 pA) with the corresponding TCNQ and TCNQ-CH_2CN on gr-Ru. arb. units, arbitrary units.

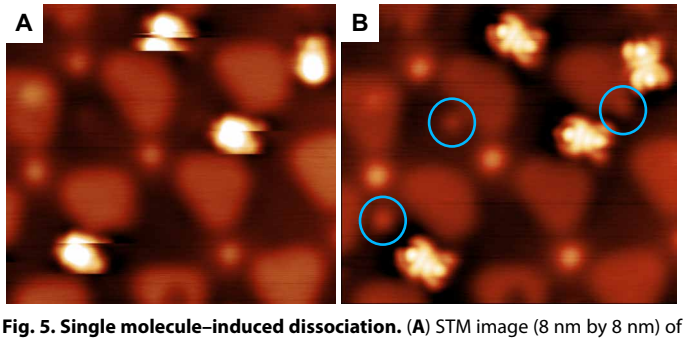

Fig. 5. Single molecule–induced dissociation. (**A**) STM image (8 nm by 8 nm) of four TCNQ-CH_2CN molecules on gr-Ru. There are also four $-CH_2CN$ groups attached to the gr-Ru (V_b = +1.7 V, I_t = 10 pA). (**B**) STM image (8 nm by 8 nm) of the same area of the sample shown in (A), acquired with the same tunneling conditions after the single-molecule manipulation process discussed in the text. Four pristine TCNQ molecules can be observed in the image. The blue circles indicate the new $-CH_2CN$ groups on the surface that appear after the C–C bond breaking induced by the injection of electrons in the LUMO of TCNQ-CH_2CN.

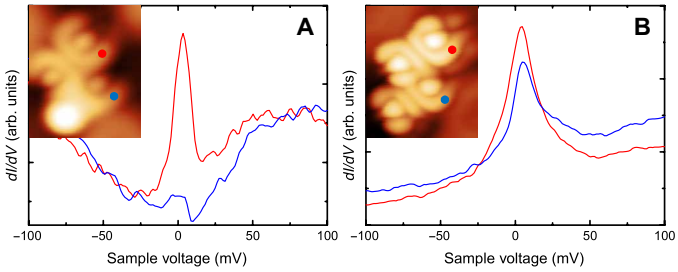

Fig. 6. Switching on the Kondo effect. LT (4.8 K) *dI*/*dV* spectra measured on the two molecules forming the dimer shown in the insets (STM images, 2.0 nm by 2.4 nm; $V_b = -0.1$V, $I_t = 20$ pA). (**A**) TCNQ and TCNQ-CH_2CN. (**B**) Two TCNQ molecules (spectra were recorded at the positions marked by the corresponding colored dots).

a bridge position (*16*). The spectrum measured with the STM tip held on top of the cyano group of the TCNQ molecule (in red) shows the Kondo resonance as expected from our previous results (*16*, *28*). In sharp contrast, the *dI*/*dV* spectrum measured in one of the pristine cyano groups of the TCNQ moiety in the TCNQ-CH_2CN is featureless (blue curve). This is the consequence of the double occupancy of the corresponding molecular orbitals. The neutral molecule in the gas phase has an odd number of electrons, but the singlet spin state is recovered thanks to the extra electron transferred from the gr-Ru to the molecule, which results in the final double occupancy of all the molecular orbitals below E_F (see section S9). Taking advantage of the reversibility of the covalent reaction, using the manipulation process described above, we removed the cyanomethylene group from the TCNQ-CH_2CN. The inset in Fig. 6B shows that the dimer, now formed by two TCNQs, is still adsorbed on the bridge position. The corresponding *dI*/*dV* spectra measured on one of the cyano groups of each TCNQ present a sharp peak at the Fermi level, implying that the reversibility of the chemical reaction can be thought of as an "on/off" switch for the Kondo effect.

In conclusion, we have shown how graphene promotes the reversible formation of a C–C bond between $-CH_2CN$ and TCNQ through three effects. First, it allows for an efficient charge transfer between the ruthenium substrate and the reactants, thus favoring changes in carbon hybridization; second, it holds the $-CH_2CN$ reactants in place and allows the reduced TCNQ to diffuse freely on the surface; and last, it avoids the reaction between the TCNQ and the Ru(0001) surface. The product of the reaction is a contorted TCNQ-CH_2CN conjugate, which, when adsorbed on gr-Ru, does not present a magnetic moment. The reaction is fully reversible by injection of electrons from the STM tip at voltages >+1.7 eV, upon which both reagents are recovered. One can think of TCNQ as a chemical "mop" with which the $-CH_2CN$ addends can be removed from the graphene surface, a cleaning operation that is otherwise impossible without decomposition of the graphene layer, even at temperatures as high as 600 K (*25*, *26*). On the other hand, the TCNQ/TCNQ-CH_2CN pair can be viewed as a reversible magnetic switch controlled by a chemical reaction. We will explore both possible applications in the near future.

MATERIALS AND METHODS

Sample preparation

The graphene layer was prepared by keeping the Ru crystal at 1150 K in UHV while exposing it to an ethylene partial pressure of 1×10^{-7} mbar for 3 min. Acetonitrile was introduced in the UHV chamber via a leak valve to produce a partial pressure of 1×10^{-6} torr during 12 min with the sample held at 374 K. TCNQ molecules were evaporated from a quartz crucible heated at 350 K with the sample held at room temperature with a deposition rate of one layer every 4 min.

STM experiments

All experiments were performed in a UHV chamber with a base pressure of 5×10^{-11} mbar equipped with an LT-STM and facilities for tip and sample preparation. The clean W tips were prepared by Ar^+ sputtering (2.5 keV) in UHV for 45 min and then heated up by resistive heating (*36*). All the STM/STS data were measured with both tip and sample at 4.8 K.

DFT calculations

The final geometry configuration and the barrier energy for the reaction in the gas phase were obtained at the MP2/6-311++G(d,p), DFT-B3LYP/6-31++G(d,p), and B3LYP/6-31G(d) theory level, respectively. These calculations have been carried out using the Quantum Chemistry package Gaussian (see the Supplementary Materials for more details). In the geometry optimization, a full relaxation of all the coordinates was carried out without imposing any condition on the symmetry of the molecule.

DFT-based adsorption studies of the TCNQ-CH_2CN molecule on gr-Ru(0001) were carried out using the Projector Augmented Wave (PAW) method as implemented in the Vienna Ab initio Simulation Package code (*37*), and we applied the Perdew-Burke-Ernzerhof exchange correlation functional, whereas weak dispersion forces were taken into account using the Tkatchenko-Scheffler method (*38*). The gr-Ru(0001) interface was modeled by a (11 × 11) graphene unit cell adsorbed on a three-layer-thick (10 × 10) Ru unit cell. In all periodic calculations, the Brillouin zone sampling was limited to the Γ point, and a strict 10^{-5}–eV convergence criterion was set for the self-consistent runs. The moiré pattern was obtained by a geometry optimization in which we optimized all the coordinates of the graphene atoms and of the topmost Ru layer until the maximum force acting on the active atoms was less than 0.01 eV/Å. The final adsorption configuration of the molecule was obtained by fully relaxing the coordinates of all the molecule and graphene atoms. The charge transfer from the substrate to the molecule was obtained by using the partitioning methods of atoms in molecules first introduced by Bader (*39*). The simulated STM images have been calculated using the Tersoff-Hamann approach (*40*), integrating the electron density in an energy window going from the Fermi energy to $E_b = e^* V_b$ and calculating the isosurface (Isov), which corresponds to a given value of the tunneling current (I_t) as given by the relation Isov ($Å^{-3}$) = $2 \times 10^{-4} \sqrt{I_t}$ (nA).

SUPPLEMENTARY MATERIALS

Supplementary material for this article is available at http://advances.sciencemag.org/cgi/content/full/4/12/eaau9366/DC1

Section S1. gr-Ru(0001) structure and growth
Section S2. TCNQ on clean Ru(0001)
Section S3. Reduced TCNQ structure
Section S4. TCNQ-CH_2CN in gas phase
Section S5. TCNQ-CH_2CN/gr-Ru(0001) adsorption configuration
Section S6. Reaction pathway
Section S7. Negative differential conductance
Section S8. TCNQ and TCNQ-CH_2CN molecular orbitals
Section S9. Molecular orbitals occupancy and Kondo effect
Section S10. Single-molecule manipulation and reaction reversibility
Fig. S1. gr-Ru(0001) moiré pattern.

REFERENCES AND NOTES

1. R. Schlögl, Carbons, in *Handbook of Heterogeneous Catalysis*, G. Ertl, H. Knözinger, F. Schüth, J. Weitkamp, Eds. (Wiley-VCH, 2008), pp 357–427.
2. E. E. Wolf, F. Alfani, Catalysts deactivation by coking. *Catal. Rev. Sci. Eng.* **24**, 329–371 (1982).
3. C. H. Bartholomew, Mechanisms of catalyst deactivation. *Appl. Catal. A* **212**, 17–60 (2001).
4. F. Besenbacher, I. Chorkendorff, B. S. Clausen, B. Hammer, A. M. Molenbroek, J. K. Nørskov, I. Stensgaard, Design of a surface alloy catalyst for steam reforming. *Science* **279**, 1913–1915 (1998).
5. J. Lu, B. Fu, M. C. Kung, G. Xiao, J. W. Elam, H. H. Kung, P. C. Stair, Coking- and sintering-resistant palladium catalysts achieved through atomic layer deposition. *Science* **335**, 1205–1208 (2012).
6. F. Bozso, G. Ertl, M. Grunze, M. Weiss, Interaction of nitrogen with iron surfaces: I. Fe(100) and Fe(111). *J. Catal.* **49**, 18–41 (1977).
7. I. C. Bassignana, K. Wagemann, J. Küppers, G. Ertl, Adsorption and thermal decomposition of ammonia on a Ni(110) surface: Isolation and identification of adsorbed NH_2 and NH. *Surf. Sci.* **175**, 22–44 (1986).
8. R. Imbhil, M. P. Cox, G. Ertl, Kinetic oscillations in the catalytic CO oxidation on Pt(100): Experiments. *J. Chem. Phys.* **84**, 3519–3534 (1986).
9. T. A. Land, T. Michely, R. J. Behm, J. C. Hemminger, G. Comsa, STM investigation of the adsorption and temperature dependent reactions of ethylene on Pt(111). *Appl. Phys. A* **53**, 414–417 (1991).
10. M.-C. Wu, Q. Xu, D. Wayne Goodman, Investigations of graphitic overlayers formed from methane decomposition on Ru(0001) and Rh(11-20) catalysts with scanning tunneling microscopy and high-resolution electron energy loss spectroscopy. *J. Phys. Chem.* **98**, 5104–5110 (1994).
11. C. Oshima, A. Nagashima, Ultra-thin epitaxial films of graphite and boron nitride on solid surfaces. *J. Phys. Condens. Matter* **9**, 1–20 (1997).
12. J. Wintterlin, M.-L. Bocquet, Graphene on metal surfaces. *Surf. Sci.* **603**, 1841–1852 (2009).
13. M. Batzill, The surface science of graphene: Metal interfaces, CVD synthesis, nanoribbons, chemical modifications, and defects. *Surf. Sci. Rep.* **67**, 83–115 (2012).
14. D. C. Elias, R. R. Nair, T. M. G. Mohiuddin, S. V Morozov, P. Blake, M. P. Hasall, A. C. Ferrari, D. W. Boukhvalov, M. I. Katsnelson, A. K. Geim, K. S. Novoselov, Control of graphene's properties by reversible hydrogenation: Evidence for graphane. *Science* **323**, 610–613 (2009).
15. W. Chen, S. Chen, D. C. Qi, X. Y. Gao, A. T. S. Wee, Surface transfer p-type doping of epitaxial graphene. *J. Am. Chem. Soc.* **129**, 10418–10422 (2007).
16. M. Garnica, D. Stradi, S. Barja, F. Calleja, C. Díaz, M. Alcamí, N. Martín, A. L. Vázquez de Parga, F. Martín, R. Miranda, Long-range magnetic order in a purely organic 2D layer adsorbed on epitaxial graphene. *Nat. Phys.* **9**, 368–374 (2013).
17. S. Barja, M. Garnica, J. J. Hinarejos, A. L. Vázquez de Parga, N. Martín, R. Miranda, Self-organization of electron acceptor molecules on graphene. *Chem. Commun.* **46**, 8198–8200 (2010).
18. A. Black, F. Jiménez, R. Bernardo-Gavito, S. Casado, D. Granados, A. L. Vázquez de Parga, Growth and characterization of 7,7,8,8-tetracyano-quinodimethane crystals on chemical vapor deposition graphene. *J. Crys. Growth* **453**, 1–6 (2016).
19. Q. H. Wang, M. C. Hersam, Room-temperature molecular-resolution characterization of self-assembled organic monolayers on epitaxial graphene. *Nat. Chem.* **1**, 206–211 (2009).
20. B. Borca, S. Barja, M. Garnica, M. Minniti, A. Politano, J. M. Rodriguez-García, J. J. Hinarejos, D. Farías, A. L. Vázquez de Parga, R. Miranda, Electronic and geometric corrugation of periodically rippled, self-nanostructured graphene epitaxially grown on Ru(0001). *New J. Phys.* **12**, 093018 (2010).
21. A. B. Preobrajenski, M. L. Ng, A. S. Vinogradov, N. Mårtensson, Controlling graphene corrugation on lattice-mismatched substrates. *Phys. Rev. B* **78**, 073401 (2008).
22. D. Stradi, S. Barja, C. Díaz, M. Garnica, B. Borca, J. J. Hinarejos, D. Sánchez-Portal, M. Alcamí, A. Arnau, A. L. Vázquez de Parga, R. Miranda, F. Martín, Role of dispersion forces in the structure of graphene monolayers on Ru surfaces. *Phys. Rev. Lett.* **106**, 186102 (2011).
23. A. L. Vázquez de Parga, F. Calleja, B. Borca, M. C. G. Passeggi Jr., J. J. Hinarejos, F. Guinea, R. Miranda, Periodically rippled graphene: Growth and spatially resolved electronic structure. *Phys. Rev. Lett.* **100**, 056807 (2008).
24. B. Borca, S. Barja, M. Garnica, D. Sánchez-Portal, V. M. Silkin, E. V. Chulkov, C. F. Hermanns, J. J. Hinarejos, A. L. Vázquez de Parga, A. Arnau, P. M. Echenique, R. Miranda, Potential energy landscape for hot electrons in periodically nanostructured graphene. *Phys. Rev. Lett.* **105**, 036804 (2010).
25. J. J. Navarro, S. Leret, F. Calleja, D. Stradi, A. Black, R. Bernardo-Gavito, M. Garnica, D. Granados, A. L. Vázquez de Parga, E. M. Pérez, R. Miranda, Organic covalent patterning of nanostructured graphene with selectivity at the atomic level. *Nano Lett.* **16**, 355–361 (2016).
26. J. J. Navarro, F. Calleja, R. Miranda, E. M. Pérez, A. L. Vázquez de Parga, High yielding and extremely site-selective covalent functionalization of graphene. *Chem. Commun.* **53**, 10418–10421 (2017).
27. C.-L. Hsu, C.-T. Lin, J.-H. Huang, C.-W. Chu, K.-H. Wei, L.-J. Li, Layer-by-layer graphene/TCNQ stacked films as conducting anodes for organic solar cells. *ACS Nano* **6**, 5031–5039 (2012).
28. M. Garnica, D. Stradi, F. Calleja, S. Barja, C. Díaz, M. Alcamí, A. Arnau, A. L. Vázquez de Parga, F. Martín, R. Miranda, Probing the site-dependent Kondo response of nanostructured graphene with organic molecules. *Nano Lett.* **14**, 4560–4567 (2014).
29. D. Maccariello, M. Garnica, M. A. Niño, C. Navío, P. Perna, S. Barja, A. L. Vázquez de Parga, R. Miranda, Spatially resolved, site-dependent charge transfer and induced magnetic moment in TCNQ adsorbed on graphene. *Chem. Mater.* **26**, 2883–2890 (2014).
30. M. Lastapis, M. Martin, D. Riedel, L. Hellner, G. Comtet, G. Dujardin, Picometer-scale electronic control of molecular dynamics inside a single molecule. *Science* **308**, 1000–1003 (2005).
31. J. Henzl, M. Mehlhorn, H. Gawronski, K.-H. Rieder, K. Morgenstern, Reversible *cis*–*trans* isomerization of a single azobenzene molecule. *Angew. Chem. Int. Ed.* **45**, 603–606 (2006).
32. S.-W. Hla, L. Bartels, G. Meyer, K.-H. Rieder, Inducing all steps of a chemical reaction with the scanning tunneling microscope tip: Towards single molecule engineering. *Phys. Rev. Lett.* **85**, 2777–2780 (2000).
33. J. Kondo, Effect of ordinary scattering on exchange scattering from magnetic impurity in metals. *Phys. Rev.* **169**, 437–440 (1968).
34. J. Li, W.-D. Schneider, R. Berndt, B. Delley, Kondo scattering observed at a single magnetic impurity. *Phys. Rev. Lett.* **80**, 2893–2896 (1998).
35. I. Fernández Torrente, K. J. Franke, J. I. Pascual, Vibrational Kondo effect in pure organic charge-transfer assemblies. *Phys. Rev. Lett.* **101**, 217203 (2008).
36. A. L. Vázquez de Parga, O. S. Hernán, R. Miranda, A. Levy Yeyati, N. Mingo, A. Martín-Rodero, F. Flores, Electron resonances in sharp tips and their role in tunneling spectroscopy. *Phys. Rev. Lett.* **80**, 357–360 (1998).
37. G. Kresse, D. Joubert, From ultrasoft pseudopotentials to the projector augmented-wave method. *Phys. Rev. B* **59**, 1758–1775 (1999).
38. A. Tkatchenko, M. Scheffler, Accurate molecular van der Waals interactions from ground-state electron density and free-atom reference data. *Phys. Rev. Lett.* **102**, 073005 (2009).
39. W. Tang, E. Sanville, G. Henkelman, A grid-based Bader analysis algorithm without lattice bias. *J. Phys. Condens. Matter* **21**, 084204 (2009).
40. J. Tersoff, D. R. Hamman, Theory and application for the scanning tunneling microscope. *Phys. Rev. Lett.* **50**, 1998–2001 (1983).
41. S. Marchini, S. Günther, J. Wintterlin, Scanning tunneling microscopy of graphene on Ru(0001). *Phys. Rev. B* **76**, 075429 (2007).
42. A. T. N'Diaye, S. Bleikamp, P. J. Feibelman, T. Michely, Two-dimensional Ir cluster lattice on a graphene moiré on Ir(111). *Phys. Rev. Lett.* **97**, 215501 (2006).
43. J. Coraux, A. T. N'Diaye, C. Busse, T. Michely, Structural coherence of graphene on Ir(111). *Nano Lett.* **8**, 565–570 (2008).
44. T. Fujita, W. Kobayashi, C. Oshima, Novel structures of carbon layers on Pt(111) surface. *Surf. Interface Anal.* **37**, 120–123 (2005).
45. D. Martoccia, P. R. Willmott, T. Brugger, M. Björck, S. Günther, C. M. Schlepütz, A. Cervellino, S. A. Pauli, B. D. Patterson, S. Marchini, J. Wintterlin, W. Moritz, T. Greber, Graphene on Ru(0001): A 25 × 25 supercell. *Phys. Rev. Lett.* **101**, 126102 (2008).
46. A. T. N'Diaye, J. Coraux, T. N. Plasa, C. Busse, T. Michely, Structure of epitaxil graphene on Ir(111). *New J. Phys.* **10**, 043033 (2008).
47. P. W. Sutter, J.-I. Flege, E. A. Sutter, Epitaxial graphene on ruthenium. *Nat. Mater.* **7**, 406–411 (2008).
48. B. Wang, S. Günther, J. Wintterlin, M.-L. Bocquet, Periodicity, work function and reactivity of graphene on Ru(0001) from first principles. *New J. Phys.* **12**, 043041 (2010).
49. B. Milián, R. Pou-Amérigo, R. Viruela, E. Ortí, On the electron affinity of TCNQ. *Chem. Phys. Lett.* **391**, 148–151 (2004).
50. R. Krishnan, J. S. Binkley, R. Seeger, J. A. Pople, Self-consistent molecular orbital methods. XX. A basis sets for correlated wave functions. *J. Chem. Phys.* **72**, 650–654 (1980).

51. C. Lee, W. Yang, R. G. Parr, Development of a Colle-Salvetti correlation-energy formula into a functional of the electron density. *Phys. Rev. B* **37**, 785–789 (1988).
52. M. J. Frisch, G. W. Trucks, H. B. Schlegel, G. E. Scuseria, M. A. Robb, J. R. Cheeseman, et al., Gaussian 09, Revision C.01, 2010, Gaussian, Inc. Wallingford CT.
53. A. D. Becke, Density-functional thermochemistry. III. The role of exact exchange. *J. Chem. Phys.* **98**, 5648–5652 (1993).
54. M. Head-Gordon, J. A. Pople, M. J. Frisch, MP2 energy evaluation by direct methods. *Chem. Phys. Lett.* **153**, 503–506 (1988).
55. T. L. Cottrell, *The Strengths of Chemical Bonds* (Academic Press/Butterworths, ed. 2, 1958).
56. M. M. Francl, W. J. Pietro, W. J. Hehre, J. S. Binkley, M. S. Gordon, D. J. DeFrees, J. A. Pople, Self-consistent molecular orbital methods. XXIII. A polarization-type basis set for second-row elements. *J. Chem. Phys.* **77**, 3654–3665 (1982).
57. A. Kondo, S. Iwatauki, Reaction of 7,7,8,8-tetracyanoquinodimethan with cyclic enol ethers. *J. Org. Chem.* **47**, 1965–1968 (1982).
58. M. Grobis, A. Wachowiak, R. Yamachica, M. F. Crommie, Tuning negative differential resistance in a molecular film. *Appl. Phys. Lett.* **86**, 204102 (2005).

Acknowledgments

Funding: J.J.N., F.C., R.M., and A.L.V.d.P. acknowledge the Ministerio de Economía y Competitividad (MINECO) project FIS2015-67367-C2-1-P and Comunidad de Madrid projects MAD2D P2013/MIT-3007 and Nanofrontmag S2013/MIT-2850. M.P., C.D., and F.M. acknowledge the MINECO project FIS2016-77889-R and computer time from the CCC-UAM and the Red Española de Supercomputación. C.D. acknowledges a Ramón y Cajal contract from MINECO (Spain). E.M.P., J.V., and B.N.-O. acknowledge the European Research Council project MINT, ERC-StG-2012-307609. IMDEA Nanoscience acknowledges support from the "Severo Ochoa" Programme for Centres of Excellence in R&D (MINECO, grant SEV-2016-0686). IFIMAC acknowledges support from the "María de Maeztu" Programme for Units of Excellence in R&D (MDM-2014-0377). **Author contributions:** J.J.N., C.G.A., and F.C. carried out the experiments. M.P., B.N.-O., and J.V. performed the calculations, with contributions from C.D. and F.M. leading the theoretical approach. E.M.P. and A.L.V.d.P. designed the experiment. J.J.N., F.C., A.L.V.d.P., and R.M. carried out the data analysis. A.L.V.d.P., E.M.P., M.P., and F.M. wrote the manuscript. All the authors discussed the manuscript. **Competing interests:** The authors declare that they have no competing interests. **Data and materials availability:** All data needed to evaluate the conclusions in the paper are present in the paper and/or the Supplementary Materials. Additional data related to this paper may be requested from the authors.

Submitted 30 July 2018
Accepted 14 November 2018
Published 14 December 2018
10.1126/sciadv.aau9366

Citation: J. J. Navarro, M. Pisarra, B. Nieto-Ortega, J. Villalva, C. G. Ayani, C. Díaz, F. Calleja, R. Miranda, F. Martín, E. M. Pérez, A. L. Vázquez de Parga, Graphene catalyzes the reversible formation of a C–C bond between two molecules. *Sci. Adv.* **4**, eaau9366 (2018).

ScienceAdvances

Graphene catalyzes the reversible formation of a C–C bond between two molecules

J. J. Navarro, M. Pisarra, B. Nieto-Ortega, J. Villalva, C. G. Ayani, C. Díaz, F. Calleja, R. Miranda, F. Martín, E. M. Pérez and A. L. Vázquez de Parga

Sci Adv **4** (12), eaau9366.
DOI: 10.1126/sciadv.aau9366